X-Ray Powder and Electron Diffraction Studies of the Average Structure and Superstructure of $BiLa_2O_{4.5}$

M. Wołcyrz,[1] L. Kępiński, and R. Horyń

Institute of Low Temperature and Structure Research, Polish Academy of Sciences, P.O. Box 937, 50-950 Wrocław, Poland

An average structure of $BiLa_2O_{4.5}$ has been determined by X-ray powder diffraction and refined by the Rietveld refinement procedure ($R3m$ space group, $a = 3.963(1)$ Å; $c = 9.964(4)$ Å; hexagonal setting). The fluorite-type structure, with the unit cell stretched along |111| direction and with oxygen atoms displaced slightly, contains statistically distributed Bi/La and O atoms. A hexagonal superstructure unit cell of $BiLa_2O_{4.5}$ ($a = 31.67$ Å, $c = 19.93$ Å), probably a consequence of oxygen ordering, has been determined by electron diffraction. A comparison of the six phases found in the Bi_2O_3–La_2O_3 system is given to indicate their common structural features. $BiLa_2O_{4.5}$ can be treated as a representative of the $Bi_3RE_5O_{12}$-type phases (RE=Y, La–Lu). © 1995 Academic Press, Inc.

INTRODUCTION

Bi_2O_3–RE_2O_3 phase diagrams (RE, rare earth) have been widely studied. To date, studies of these systems have focused on Bi-rich regions, because fluorite-type δ-Bi_2O_3 and its numerous δ*-type solid-solutions with dilute concentrations of other metal oxides (e.g., Y_2O_3 or Ln_2O_3; Ln = Sm–Yb (1)) have high ionic conductivity. According to the data available, doping of Bi_2O_3 with oxides of larger cations (e.g., La_2O_3 or SrO) produces rhombohedral solid-solutions. Their typical representatives are $Bi_{0.765}Sr_{0.235}O_{1.383}$ (2) and $Bi_{0.7}La_{0.3}O_{1.5}$ (3). Little is known about Ln-rich compositions in Bi_2O_3-systems except the $Bi_8La_{10}O_{27}$ phase reported in (4).

In a previous paper (5) we reported the existence of a series of RE-based bismuth oxides (RE=Y, La–Lu) stable in air. These oxides have a comparatively wide compositional range extending from the $Bi_3RE_5O_{12}$ stoichiometry. Among them, the La representative was exceptional, exhibiting $BiLa_2O_{4.5}$ stoichiometry. Its unique position comes from the fact that within the Bi_2O_3–La_2O_3 binary system, very close to the 3:5 stoichiometry, there is a neighboring $Bi_8La_{10}O_{27}$ phase. Accordingly, the chemical composition of the La representative of our series is shifted from 3:5 to 1:2.

[1] To whom correspondence should be addressed.

In (5) we dealt with the crystallochemical characterization of the $Bi_3RE_5O_{12}$ series as a whole. In this paper we concentrate on a more detailed crystallographic description of $BiLa_2O_{4.5}$. In spite of a certain peculiarity concerning the stoichiometry, $BiLa_2O_{4.5}$ has many similarities with the other $Bi_3RE_5O_{12}$ phases and can be treated as their representative. We also compare all phases known-to-date of the Bi_2O_3–La_2O_3 system in order to indicate their common structural features.

EXPERIMENTAL

Samples were prepared from Johnson Mathey's La_2O_3 and Bi_2O_3, both of 4N purity. The preparation consisted of heating the appropriate mixtures of the oxides in air at 800°C for 24 hr, then regrinding, pelletizing, and subsequently heating at 900°C for 48 hr. Final sintering of the products was performed at 950°C for 3 days. For some test samples, sintering was restricted to 900°C/48 hr. Powders were characterized by X-ray powder diffraction (Siemens D 5000 diffractometer, Ni-filtered CuKα radiation) and transmission electron microscopy (Philips CM 20 SuperTwin microscope operating at 200 kV), where bright field images and selected area electron diffraction patterns (SAED) were recorded. Sample density was measured pycnometrically with CCl_4 as the immersion medium.

RESULTS AND DISCUSSION

Phase Relations in the Bi_2O_3–La_2O_3 System at 900°C

Several samples with different Bi/La ratios ($Bi_2LaO_{4.5}$, $BiLaO_3$, $Bi_4La_5O_{13.5}$, $Bi_2La_3O_{7.5}$, $Bi_3La_5O_{12}$, $Bi_4La_7O_{16.5}$, and $BiLa_2O_{4.5}$) have been prepared and analyzed by X-ray powder diffraction. The results obtained, together with the previous findings reported in (2–4), allowed us to construct a tentative 900°C isothermal section through the Bi_2O_3–La_2O_3 system (Fig. 1). Phases found and their mutual relations are the following:

(i) fluorite-like δ-Bi_2O_3 stable above 730°C, $Fm3m$ space group, $a = 5.660$ Å (JCPDS Card 16-654);

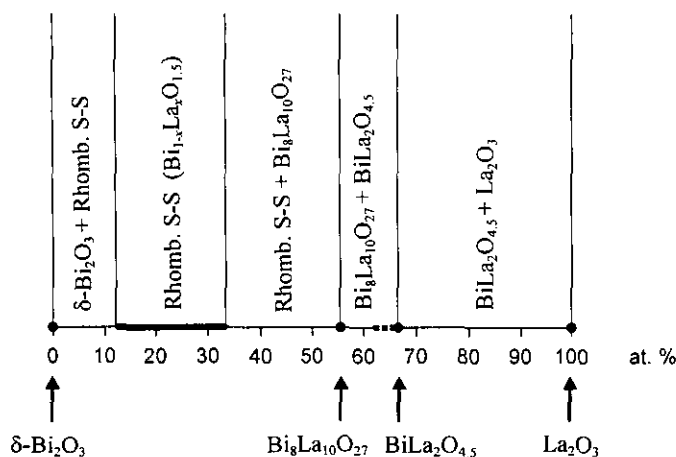(ii) rhombohedral $Bi_{1-x}La_xO_{1.5}$ solid solution (~0.12 ≤

FIG. 1. Phase relations in the Bi$_2$O$_3$–La$_2$O$_3$ system in air at 900°C.

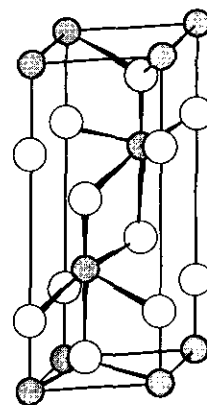
FIG. 3. A hexagonal subcell of BiLa$_2$O$_{4.5}$. Shaded circles, Bi/La atoms; open circles, O atoms.

$x \leq 0.333$), $R\overline{3}m$ space group, $a = 4.043$ Å and $c = 27.557$ Å (hexagonal setting) for Bi$_{0.7}$La$_{0.3}$O$_{1.5}$ (3);

(iii) stoichiometric Bi$_8$La$_{10}$O$_{27}$ phase, *Immm* space group, $a = 12.079$ Å, $b = 16.348$ Å, and $c = 4.098$ Å (4);

(iv) BiLa$_2$O$_{4.5}$, the phase under discussion. Most probably a stoichiometric phase, but possibly extending slightly toward Bi-rich compositions (>36 at.% Bi).

(v) La$_2$O$_3$, *P3m1* space group, $a = 3.937$ Å and $c = 6.130$ Å (JCPDS Card 5-602).

Average Structure of BiLa$_2$O$_{4.5}$

The stoichiometry of BiLa$_2$O$_{4.5}$ is shifted from the common location, characteristic of other *RE*-based bismuth oxides, i.e., from 3 : 5 : 12. Its density ($d_m = 6.83$ g/cm^3, $d_x = 6.86$ g/cm^3) justifies the BiLa$_2$O$_{4.5}$ composition.

Figure 2a shows X-ray powder diffraction diagram of BiLa$_2$O$_{4.5}$ (peak positions are collected in Table 1). Taking into account strong peaks only, the diagram can be indexed in a rhombohedral cell ($a_H = 3.963(1)$ Å; $c_H = 9.964(4)$ Å; hexagonal setting) but several weak, unin-
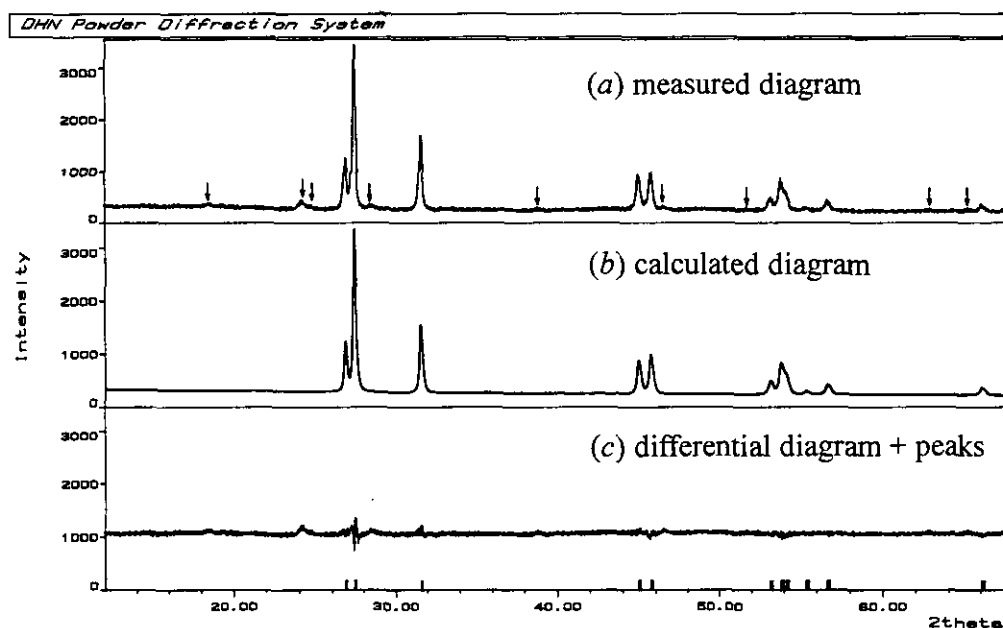

FIG. 2. Results of the Rietveld refinement of the average structure of BiLa$_2$O$_{4.5}$: (a) measured diagram, (b) calculated diagram, and (c) differential diagram. Arrows mark weak superstructure peaks absent for the average structure model.

TABLE 1

Observed Interplanar Spacings (d_{obs}), Bragg angles ($2\Theta_{obs}$), and Relative Intensities (I_{rel}) for BiLa$_2$O$_{4.5}$ (cf. Fig. 1) Compared with the Calculated Values for the Refined Superstructure Cell ($a = 31.672$ Å, $c = 19.927$ Å)

d_{obs} (Å)	d_{calc} (Å)	$2\Theta_{obs}$ (°)	$2\Theta_{calc}$ (°)	I_{rel} (%)	hkl_H	hkl_{sup}
4.748	4.752	18.67	18.66	4.4		1 1 4
3.666	3.664	24.25	24.27	6.0		5 2 3
3.590	3.592	24.77	24.76	4.1		4 2 4
3.320	3.321	26.83	26.82	30.1	0 0 3	0 0 6
3.240	3.242	27.50	27.49	100.0	1 0 1	8 0 2
3.126	3.128	28.52	28.51	3.6		5 5 1
2.866	2.866	31.18	31.18	4.7		8 2 2
2.823	2.824	31.66	31.65	46.8	1 0 2	8 0 4
2.396	2.397	37.50	37.48	2.0		8 5 1
2.015	2.015	44.94	44.94	25.6	1 0 4	8 0 8
1.979	1.979	45.80	45.80	27.8	1 1 0	8 8 0
1.947	1.947	46.61	46.60	3.8		9 5 5
1.755	1.754	52.07	52.09	0.8		9 1 9
1.722	1.723	53.13	53.12	10.7	1 0 5	8 0 10
1.700	1.700	53.87	53.87	21.3	1 1 3	8 8 6
1.689	1.689	54.26	54.25	9.0	2 0 1	16 0 2
1.661	1.660	55.26	55.28	2.0		10 9 1
1.621	1.621	56.74	56.74	8.2	2 0 2	16 0 4
1.473	1.473	63.04	63.03	1.0		7 9 9
1.423	1.423	65.52	65.53	1.2	0 0 7	0 0 14
1.412	1.412	66.11	66.11	6.0	2 0 4	16 0 8

Note. Miller indices given for the subcell (hkl_H) and superstructure cell (hkl_{sup}).

TABLE 2

Details of the Rietveld Refinement of the Average Structure of BiLa$_2$O$_{4.5}$

2Θ range (°)	10–70
Step-scan size (°)	0.02
Number of points	3001
Profile shape	Pearson VII
Number of profile parameters	12
Number of structure parameters	4

Space group: $R3m$ (hexagonal setting); $Z = 1$; $a = 3.963(1)$ Å; $c = 9.964(4)$ Å

Atom	Position	x	y	z	B (Å^2)	Occupation
Bi	3(a)	0	0	0	0.6	0.333
La	3(a)	0	0	0	0.6	0.667
O1	3(a)	0	0	0.215(1)	1.0	0.75
O2	3(a)	0	0	0.723(1)	1.0	0.75

Fixed parameters	temperature factors, occupation
Scale factor	$0.322(2) \times 10^{-5}$
Half width coefficients (U, V, W)	0, 0.12003(83), 0.00827(22)
Profile shape parameter m	1.42(2)
Preferred orientation parameter (March–Dollase function)	0.981(7)
Preferred orientation direction	[001]
Discrepancy factors	$R_p = 0.064$; $R_{wp} = 0.081$; $R_B = 0.052$

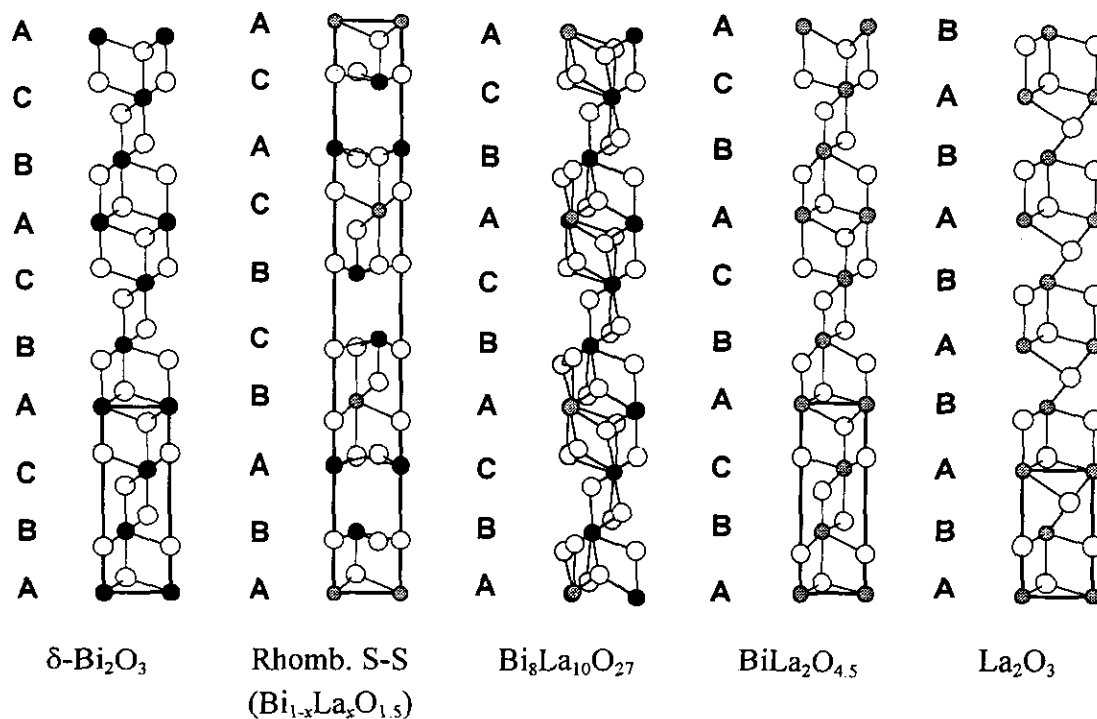*Note.* Half-widths are calculated according to the formula HW = $\sqrt{U \tan^2 \Theta + V \tan \Theta + W}$.

δ-Bi$_2$O$_3$ Rhomb. S-S (Bi$_{1-x}$La$_x$O$_{1.5}$)   Bi$_8$La$_{10}$O$_{27}$ BiLa$_2$O$_{4.5}$ La$_2$O$_3$

FIG. 4. Comparison of the crystal structures known in the Bi$_2$O$_3$–La$_2$O$_3$ system: δ-Bi$_2$O$_3$; Bi$_{0.7}$La$_{0.3}$O$_{1.5}$; Bi$_8$La$_{10}$O$_{27}$; BiLa$_2$O$_{4.5}$; La$_2$O$_3$. Pictures present a structure projection on ($\bar{1}20$) crystallographic plane of the appropriate hexagonal lattice. Full circles, Bi atoms; shaded circles, Bi/La atoms; open circles, O atoms. Capital letters denote layers of metal atoms. Comparable hexagonal unit cells are marked by bold lines, where possible.

dexed peaks indicate a possible superstructure. However, their negligible intensities (probably due to slight structure reconstruction) make the crystal structure refinement in the rhombohedral subcell quite reasonable. We decided to perform the calculations for a simple structural model applied in (6) for BiO thin film, but with an additional position for the access of oxygen. Such a structure can be interpreted as fluorite type with the unit cell stretched along the [111] direction and with oxygen atoms slightly displaced (Fig. 3). Atoms of all the structure components occupy three different positions in the unit cell of $R3m$ space group. The first one is occupied statistically by Bi and La atoms, and the remaining two positions contain statistically distributed oxygen. The results of the Rietveld refinement performed with the DBWS-9006PC program (7) are collected in Table 2 and presented graphically in Figs. 2b and 2c. Bond lengths are collected in Table 3. They are in a good agreement with data known for bismuth oxides and Bi$_2$O$_3$–La$_2$O$_3$ ternary phases.

Figure 4 shows a comparison of the structures in the system: fluorite-type δ-Bi$_2$O$_3$, rhombohedral Bi$_{0.7}$La$_{0.3}$O$_{1.5}$, orthorhombic Bi$_8$La$_{10}$O$_{27}$, rhombohedral BiLa$_2$O$_{4.5}$, and finally hexagonal La$_2$O$_3$. All these structures originate from a close packing of the metal-atom layers with oxygen atoms between them. Cubic, fcc-lattice-forming packing of δ-Bi$_2$O$_3$ with an A–B–C layer sequence and, on the opposite side, hcp-lattice-forming A–B packing of La$_2$O$_3$, constitute a frame for all the structures under discussion. In between one can find a complex A–B–A–B–C–B–C–A–C–A packing characteristic for Bi$_{0.7}$La$_{0.3}$O$_{1.5}$ structure and A–B–C packings for Bi$_8$La$_{10}$O$_{27}$ and BiLa$_2$O$_{4.5}$. However, in the last two cases, homogeneous, equiatomic layers of metal atoms do not exist. In Bi$_8$La$_{10}$O$_{27}$, which forms a relatively complex and strongly distorted structure, the layers are deformed and contain both Bi and La atoms ordered in a specific way. In the case of BiLa$_2$O$_{4.5}$ the model with the statistical distribution of atoms proposed by us is quite satisfactory for the description of the average structure.

Electron Microscopy Studies

SAED technique has provided a number of reciprocal lattice sections of BiLa$_2$O$_{4.5}$. Three of them are presented

TABLE 3

Bond Lengths (Å)
for the Average Structure of BiLa$_2$O$_{4.5}$

Bi(La)–O1	2.14
	2.57
Bi(La)–O2	2.36
	2.76
O1–O2	2.78
	2.88
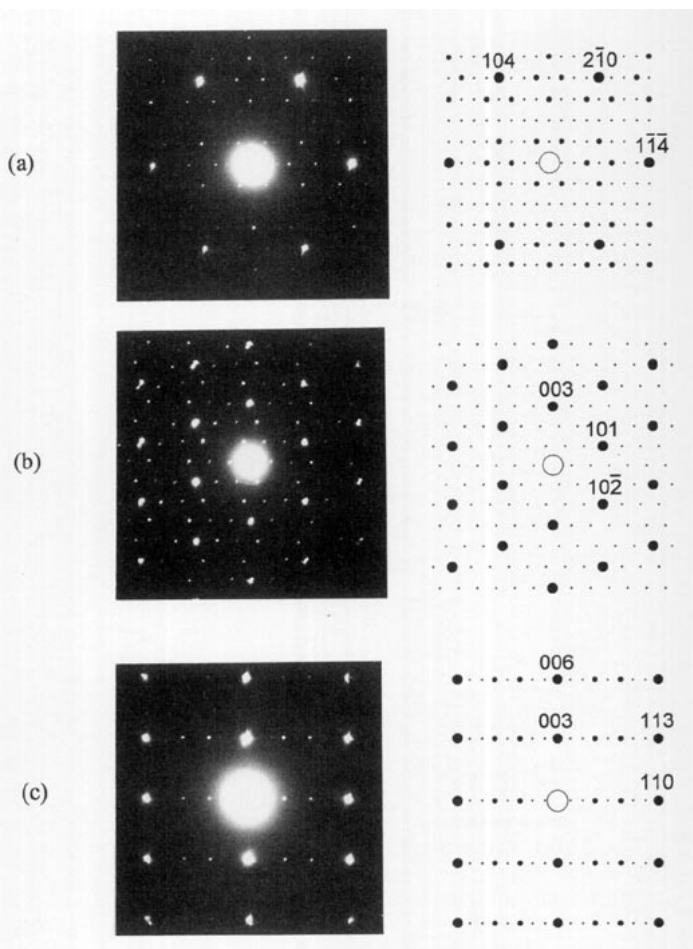
FIG. 5. SAED patterns of BiLa$_2$O$_{4.5}$. Electron beam parallel to the (a) [48$\bar{1}$], (b) [010], and (c) [1$\bar{1}$0] zone axis. Reflections coming from the average structure are indexed according to the hexagonal subcell.

in Fig. 5. Strong reflections, originating from the average structure, are indexed in the hexagonal subcell. Between them, many weak superstructure spots are located. An indexing procedure, similar to the autoindexing routine commonly applied in the single crystal X-ray diffractometry, was used in order to find the superstructure unit cell. As a result, a hexagonal cell has been obtained with $a = 31.67$ Å and $c = 19.93$ Å. A relation between superstructure $(\mathbf{a}, \mathbf{c})$ and average structure lattice vectors $\mathbf{a}_H$, $\mathbf{c}_H$) is $\mathbf{a} = 8 \cdot \mathbf{a}_H$, $\mathbf{c} = 2 \cdot \mathbf{c}_H$. The multiple cell $(8a_H \times 8a_H \times 2c_H)$ has allowed to index all observed X-ray powder diffraction peaks (cf. Table 1).

Figure 6 shows high-resolution electronmicrograph of BiLa$_2$O$_{4.5}$ crystal oriented with its [42$\bar{1}$] direction parallel to the electron beam (note that all indices are applied according to the hexagonal subcell of the rhombohedral lattice appropriate for the average structure). The overall symmetry of the image is in reasonable agreement with the projection of the crystal structure on the ($\bar{1}$02) lattice plane (Fig. 6, inset). The square lattice of white dots ($a \cong 2.7$ Å) harmonizes with the knots of the fluorite-type
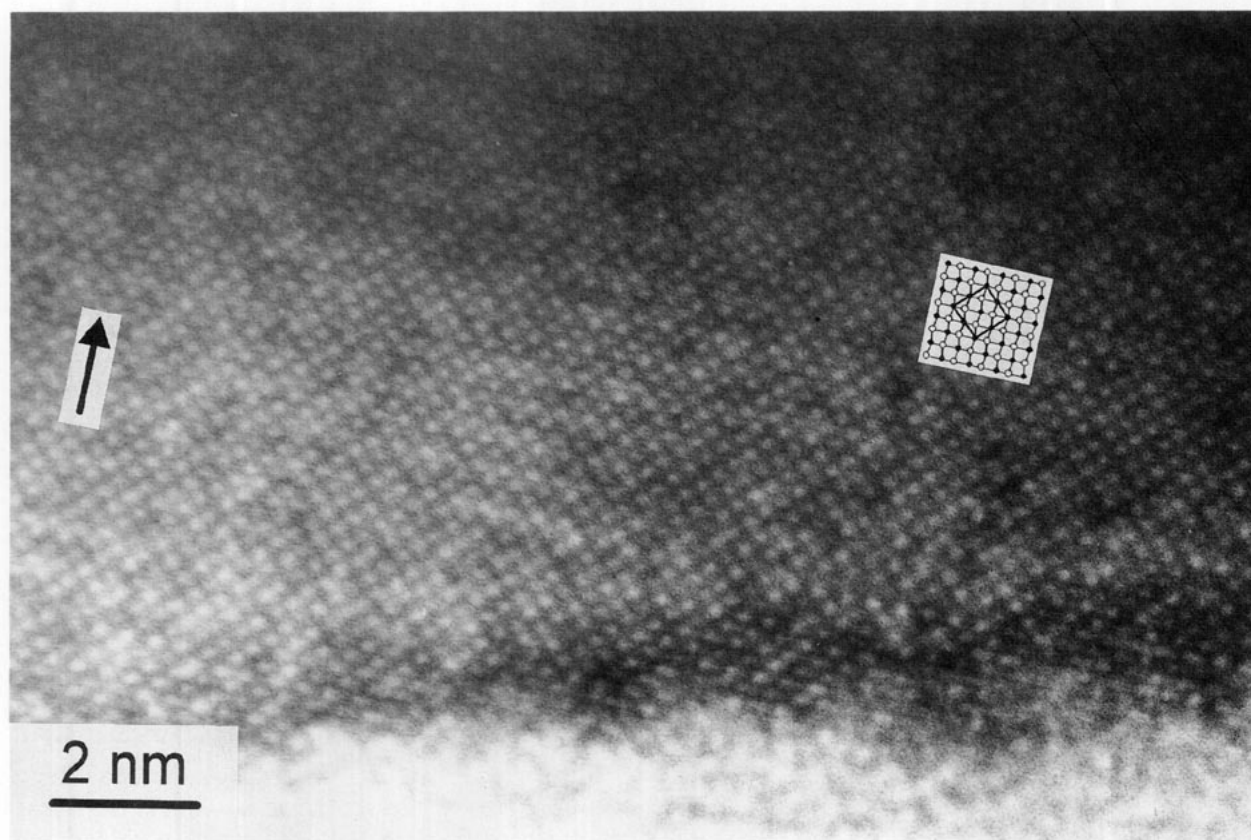
FIG. 6. High-resolution electron micrograph and corresponding projection of the crystal lattice (inset) of $BiLa_2O_{4.5}$ crystal oriented with its [42$\bar{1}$] direction parallel to the electron beam. The fluorite-type unit cell is marked with bold lines. The arrow indicates the [010] direction, perpendicular to the superstructure features.

lattice. Along the crystal image, perpendicularly to the [010] direction, features with longer periodicity are visible. These correspond to the superstructure.

A full explanation of the superstructure is not possible at this stage of the investigation. However, some general remarks can be given. In order to describe the superstructure, it is necessary to allow for ordering of oxygen or, maybe, also metal atoms. However, ordering effects in $BiLa_2O_{4.5}$ are distinctly weaker than those in $Bi_8La_{10}O_{27}$ or $Bi_{0.7}La_{0.3}O_{1.5}$. This indicates that rather subtle ordering phenomena take place, referred most probably to oxygen atoms, without inducing a strong lattice distortion due to the metal atoms ordering. Single crystal studies should supply a definite solution.

REFERENCES

1. D. Mercurio, M. El Farissi, and B. Frit, *Solid State Ionics* **39**, 297 (1990).
2. P. Conflant, J.-C. Boivin, and D. Thomas, *J. Solid State Chem.* **35**, 192 (1980).
3. D. Mercurio, M. El Farissi, J. C. Champarnaud-Mesjard, and B. Frit, *J. Solid State Chem.* **80**, 133 (1989).
4. C. Michel, V. Caignaert, and B. Raveau, *J. Solid State Chem.* **90**, 296 (1991).
5. R. Horyń, M. Wołcyrz, and A. Wojakowski, *J. Solid State Chem.* **116**, 68 (1995).
6. A. A. Zavyalova, R. M. Imamov, and Z. G. Pinsker, *Kristallografiya*, **10**, 480 (1965).
7. A. Sakthivel and R. A. Young, "Program DBWS-9006PC for Rietveld Analysis of X-ray and Neutron Powder Diffraction Patterns." Release of August 12, 1991.